

Graphene Oxide Interlayers for Robust, High-Efficiency Organic Photovoltaics

Ian P. Murray,^{†,‡} Sylvia J. Lou,^{‡,§} Laura J. Cote,[†] Stephen Loser,^{‡,§} Cameron J. Kadleck,^{†,‡} Tao Xu,^{‡,⊥} Jodi M. Szarko,^{‡,§} Brian S. Rolczynski,^{‡,§} James E. Johns,[†] Jiaxing Huang,[†] Luping Yu,^{*,†,‡,⊥} Lin X. Chen,^{*,‡,§,||} Tobin J. Marks,^{*,†,‡,§} and Mark C. Hersam^{*,†,‡,§,#}

[†]Department of Materials Science and Engineering, Northwestern University, Evanston, Illinois 60208, United States

[‡]Argonne Northwestern Solar Energy Research Center, Evanston, Illinois 60208, United States

[§]Department of Chemistry, Northwestern University, Evanston, Illinois 60208, United States

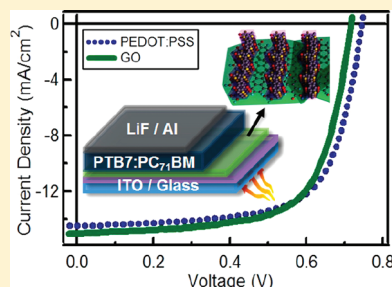
^{||}Chemical Science and Engineering Division, Argonne National Laboratory, Argonne, Illinois 60439, United States

[⊥]Department of Chemistry, University of Chicago, Chicago, Illinois 60637, United States

[#]Department of Medicine, Northwestern University, Evanston, Illinois 60208, United States

 Supporting Information

ABSTRACT: Organic photovoltaic (OPV) materials have recently garnered significant attention as enablers of high power conversion efficiency (PCE), low-cost, mechanically flexible solar cells. Nevertheless, further understanding-based materials developments will be required to achieve full commercial viability. In particular, the performance and durability of many current generation OPVs are limited by poorly understood interfacial phenomena. Careful analysis of typical OPV architectures reveals that the standard electron-blocking layer, poly-3,4-ethylenedioxy-thiophene:poly(styrene sulfonate) (PEDOT:PSS), is likely a major factor limiting the device durability and possibly performance. Here we report that a single layer of electronically tuned graphene oxide is an effective replacement for PEDOT:PSS and that it significantly enhances device durability while concurrently templating a performance-optimal active layer π -stacked face-on microstructure. Such OPVs based on graphene oxide exhibit PCEs as high as 7.5% while providing a 5× enhancement in thermal aging lifetime and a 20× enhancement in humid ambient lifetime versus analogous PEDOT:PSS-based devices.



SECTION: Energy Conversion and Storage

Organic photovoltaics (OPVs) have attracted great interest as low-cost, mechanically flexible sources of solar power.^{1–6} While the historical focus has been on power conversion efficiency (PCE), acceptable durability will also be required for OPVs to become a viable technology.^{7–10} A primary weakness of bulk heterojunction (BHJ) OPVs is instability at the interface between the indium tin oxide (ITO) anode and the hole-extracting interfacial layer (IFL).^{11–13} The canonical IFL, poly-3,4-ethylenedioxy-thiophene:poly(styrene sulfonate) (PEDOT:PSS), is often implicated in processes that limit efficiency and ultimately lead to OPV failure.^{11,14,15} Graphene oxide (GO) is a robust, mechanically flexible and electronically tunable hole-transporting material with many properties suggestive of an effective OPV IFL.^{16–19} We report here that, for a state-of-the-art BHJ active layer material, GO both templates an active layer microstructure that optimizes performance and significantly enhances device lifetime. Importantly, OPVs fabricated with ITO/single-layer GO exhibit PCEs as high as 7.5% with a 5× enhancement in thermal aging lifetime and a 20× enhancement in humid ambient lifetime versus comparable PEDOT:PSS devices.

BHJ OPVs combining the well-characterized and well-documented electron donating polymer poly[[4,8-bis[(2-ethylhexyl)oxy]benzo[1,2-b:4,5-b']dithiophene-2,6-diyl][3-fluoro-2-[(2-ethylhexyl)carbonyl]-thieno[3,4-b]thiophenediyl]] (**PTB7**; Figure 1a) and the fullerene electron acceptor [6,6]-phenyl-C₇₁-butyric-acid-methyl-ester (**PC₇₁BM**; Figure 1a) have achieved PCEs exceeding 7.5% with the active layer cast on PEDOT:PSS as the anode IFL.^{20,21} While this efficiency level is currently state-of-the-art, the performance of **PTB7** devices and many other BHJ OPV systems is limited by, among other factors, the corrosive, inhomogeneous structural and electrical properties of PEDOT:PSS.^{11,14,15} Thus, substantial research has been devoted to alternative polymeric, cross-linking, self-assembling, and inorganic IFL materials as PEDOT:PSS replacements.^{16,22–26}

Previous reports suggest that the performance of **PTB7**-based OPVs benefits substantially from a face-on oriented π -stacking of

Received: November 11, 2011

Accepted: November 12, 2011



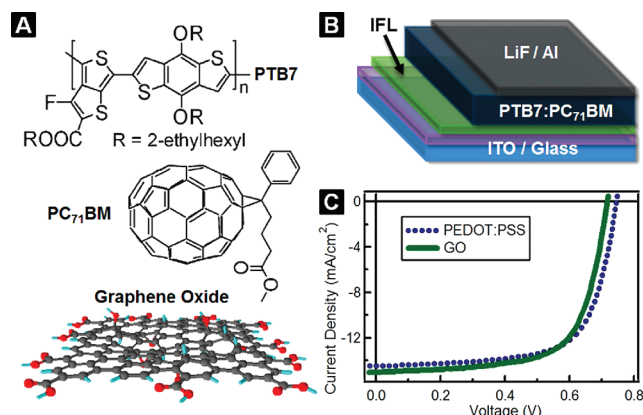


Figure 1. Comparative photovoltaic performance of PTB7:PC₇₁BM OPVs with PEDOT:PSS or GO IFLs. (a) Chemical structures of the PTB7 donor polymer, PC₇₁BM acceptor, and GO IFL.^{21,31} (b) Schematic of a standard OPV indicating the location of the IFLs. (c) Representative current–voltage plots under AM 1.5G solar simulated light for OPVs fabricated with PEDOT:PSS and GO IFLs.

the PTB7 chains at the interface with the PEDOT:PSS IFL.^{27,28} This ordered π -stacking is thought to promote efficient electronic coupling of the active layer polymer to the hole-extracting IFL/anode and to co-organize the electron conducting pathways of the intercalated PC₇₁BM networks.²⁹ Consequently, next-generation OPV IFL materials must overcome the corrosive and other undesirable properties of PEDOT:PSS while ideally templating active layer growth on the cell anode for optimum carrier extraction.

In this report, we show that, utilizing novel solution-processing techniques,^{30–32} bulk synthesized GO flakes can be deposited as films in controlled densities on ITO anodes while offering significantly greater transparency than PEDOT:PSS. These GO films, composed of overlapped monolayers, can be chemically manipulated to achieve oxidation levels compatible with efficient hole-extracting IFLs for high-PCE PTB7:PC₇₁BM-based OPVs. The microstructures of PTB7:PC₇₁BM active layers deposited on GO and PEDOT:PSS are compared here by grazing incidence X-ray scattering (GIXS) techniques, showing that GO more effectively templates the PTB7 π -stacking orientation favorable for charge extraction.²⁸ Furthermore, a recombination current analysis of the current–voltage (J – V) data argues that ideal GO layers should significantly outperform PEDOT:PSS in BHJ devices. Finally, OPVs fabricated on GO are shown here to have far greater thermal and ambient stability than those fabricated on PEDOT:PSS.

GO flakes were produced by oxidative chemical exfoliation of graphite powders, affording suspensions of large single flakes with relatively uniform oxidation levels (see Experimental Section and Supporting Information). These flakes were then deposited in controlled densities onto clean ITO substrates via Langmuir–Blodgett (LB) assembly^{30,32} (see Figure S1 for scanning electron micrographs of GO deposited on ITO). Previous work suggests that GO oxidation levels can be used to tune electronic properties,^{31,33} so variable durations of low-level ozone exposure were employed to modify the GO surface chemistry (see Experimental Section). X-ray photoelectron spectroscopy (XPS) and Raman spectroscopy confirm that the GO structure remains intact after LB deposition and ozone processing (see Figures S2 and S3).

Figure 1 summarizes the OPV architecture and performance data for devices fabricated by parallel processing of PTB7:PC₇₁BM active layers on identical ITO substrates with PEDOT:PSS or GO IFLs. The current density–voltage (J – V) characteristics are similar for each device type and result in nearly identical PCEs of 7.46% and 7.39% for PEDOT:PSS and GO, respectively (Figure 1c). Table 1 compiles a statistical analysis of 16 devices with each IFL showing reproducible differences in the short circuit current (J_{sc}) and open circuit voltage (V_{oc}).

To explore the origins of the differences/similarities in device performance, the surface morphology of each IFL was investigated. Figure 2 presents tapping-mode atomic force microscopy (AFM) images of the PEDOT:PSS and GO films on ITO substrates. Note the significant vertical scale differences in the two images, which illustrate the very different surface roughnesses of the two IFLs. In particular, the PEDOT:PSS film (Figure 2a) exhibits an overall root-mean-square (rms) roughness of 3.5 nm, whereas Figure 2b reveals a substantially lower rms roughness of 0.7 nm for the LB-derived GO films. The GO AFM image also reveals some inhomogeneity in the form of flake edges and wrinkles.

After characterizing the IFL morphology, the relative structural ordering of the PTB7:PC₇₁BM active layer films on the PEDOT:PSS and GO IFLs was quantified using GIXS techniques. Figure 3a provides a schematic of the two-dimensional (2D) data collected (see Figures S4, S5, and S6 for measurement geometry and full 2D plates). Using previously discussed data acquisition and analysis procedures,^{27,28} GIXS was used to analyze the face-on and edge-on character of the PTB7 π -chains relative to the IFL surface (see Figure 3b). To simplify the data presentation, horizontal and vertical linecuts are extracted from the 2D images. Figure 3c overlays the horizontal linecuts collected from each active layer deposited on the ITO/PEDOT:PSS and ITO/GO substrates. Two distinct scattering features are evident in this linecut, labeled **h1** and **h2**. Peak **h1** corresponds to a d -spacing of 1.9 nm, while peak **h2** is broader than **h1** and corresponds to a 0.45 nm spacing. Similar to Figure 3c, Figure 3d overlays the vertical linecuts of the 2D GIXS data for comparison. This linecut contains three scattering features, labeled **v1**, **v2**, and **v3**, each corresponding to a different length-scale or material within the sample. Features **v1** and **v2** are similar to peaks **h1** and **h2**, and correspond to average periodicities of 1.7 and 0.45 nm, respectively. Finally, the shoulder indicated as **v3** in Figure 3d corresponds to a periodicity of 3.8 Å and is enhanced on the GO substrate.

To gain further insight into the relative OPV performance of the PEDOT:PSS and GO IFLs, optical transmission spectra and external quantum efficiency (EQE) data were recorded for the OPVs as a function of illumination wavelength (Figure 4a). The transmission spectra show that across the entire visible spectrum, GO is significantly more transparent than the standard thickness PEDOT:PSS IFL used in OPVs. In terms of EQE, devices fabricated with GO IFLs significantly out-perform those fabricated with PEDOT:PSS IFLs in the 430–700 nm wavelength range. The recombination current for each device was next calculated as the differential voltage dependence of the light and dark J – V data via the equation shown in Figure 4b.³⁴ The resulting data in Figure 4b reveal that the OPVs fabricated with PEDOT:PSS IFLs have lower recombination currents than those fabricated with GO at the relevant operating potentials.

The relative durability of OPVs fabricated with either GO or PEDOT:PSS IFLs was next quantified in thermal and humid

Table 1. Photovoltaic Performance Parameters for OPVs Fabricated with Either PEDOT:PSS or GO IFLs (16 Devices for Each IFL)^a

IFL	J_{sc} (mA/cm ²)	$\sigma_{J_{sc}}$	V_{oc} (V)	$\sigma_{V_{oc}}$	FF (%)	σ_{FF}	η (%)	σ_{η}
PEDOT:PSS	-14.55	0.0683	0.741	0.0019	68.10	0.6179	7.46	0.0857
GO	-15.21	0.0239	0.716	0.0021	67.70	0.3627	7.39	0.0497

^a Average short circuit current (J_{sc}), open circuit voltage (V_{oc}), fill factor (FF), and efficiency (η) are given along with derived standard deviations (σ).

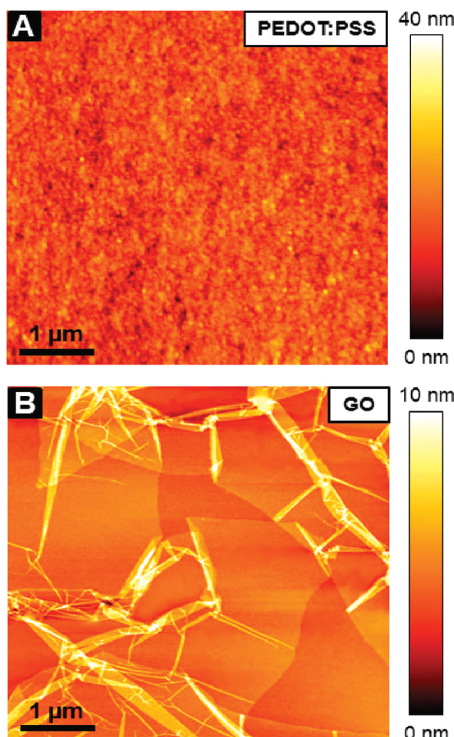


Figure 2. AFM images illustrating the different film morphologies of the PEDOT:PSS and GO IFLs. (a) AFM image of a spin-cast and annealed PEDOT:PSS film with an rms roughness of 3.5 nm. (b) AFM image of a GO film deposited by LB assembly, annealed, and treated with UV ozone (UVO) having an rms roughness of 0.7 nm.

ambient lifetime measurements. The lifetime data in Figure 5 clearly indicate that the GO IFL devices are significantly more durable than those with PEDOT:PSS IFLs. Figure 5a shows the PCE time dependence of encapsulated GO- and PEDOT:PSS-based devices held at 80 °C under inert atmosphere. The initial short time scale degradation is followed by a quasi-linear decay in both device types. By extrapolating the linear portion of each plot to zero current, lifetimes to failure of 1428 and 7156 h are extracted for the devices utilizing PEDOT:PSS and GO IFLs, respectively. Figure 5b illustrates data collected from unencapsulated devices fabricated with TiO_x/Ag cathodes that have been shown to impart greater air-stability than conventional electrodes.³⁵ When exposed to 80% relative humidity at room temperature, the devices fabricated with GO IFLs maintain PCE for significantly longer time scales than those fabricated with PEDOT:PSS IFLs. By linearly extrapolating the GO degradation data, lifetimes to failure of 6 and 122 h are extracted for the PEDOT:PSS and GO devices, respectively.

While the $J-V$ data in Figure 1 suggest that OPVs fabricated with GO and PEDOT:PSS IFLs perform equivalently, deeper examination reveals several distinct attractions of GO for PV

applications. Thus, the present results show that GO IFLs template PTB7 face-on oriented π -stacking more effectively, are more transparent in the key spectral regions, and significantly extend device lifetime under accelerated degradation conditions versus comparable devices fabricated with PEDOT:PSS IFLs.

Analysis of the GIXS data (Figure 3) shows enhanced face-on ordering of the PTB7 stacks on GO substrates. The peak **h1** d -spacing of 1.9 nm, which is strong for both GO and PEDOT:PSS, is the characteristic interchain spacing between stacked PTB7 chains oriented face-on to the substrate surface.²⁷ As noted above, this orientation is favorable for photogenerated hole extraction, and the relative intensity of this GIXS feature quantifies the degree of orientation within each active layer. Peak **v1** corresponds to a periodicity of 1.7 nm between the PTB7 chains and is more pronounced in the PEDOT:PSS samples. This vertical direction scattering intensity indicates a higher percentage of PTB7 chains with edges oriented perpendicular to the substrate surface, which correlates with reduced charge extraction by the anode.²⁸

The broader **h2** and **v2** peaks are characteristic of the (111) reflection from PC₇₁BM assemblies²⁷ and are of equal intensity for both PEDOT:PSS and GO IFLs. The absence of a strong (311) reflection at $q = 0.7$ suggests that the PC₇₁BM molecules are weakly ordered and intercalated between the PTB7 stacks. This intercalation is enhanced by the addition of 1,8-diiodooctane to the active layer spin-coating solution, allowing the PTB7 stacks to form without disruption by PC₇₁BM aggregates, thereby enhancing OPV performance.²⁹ The GIXS feature labeled **v3** in Figure 3d represents the characteristically weak signal from the $\pi-\pi$ interchain spacing of face-on PTB7 stacks. This scattering feature is enhanced on the GO substrates, demonstrating a greater preponderance of face-on PTB7 assembly on GO versus PEDOT:PSS, where **v3** is obscured by the **v2** peak.

Beyond more efficient PTB7 stacking, Figure 4a shows that GO offers greater light transmission which, all other factors being equal, should scale linearly with EQE at the corresponding wavelengths.³⁵ Figure 4a shows that the GO-based device indeed exhibits increased current generation, however, not as much as might be expected from the optical transmission data alone. One explanation for this apparent discrepancy is related to the recombination of free charge carriers near the ITO anode, quantified in Figure 4b. It has been shown that electronically homogeneous charge-blocking surfaces can enhance both OPV short-circuit current and open circuit voltage by suppressing recombination currents,^{22–24,33} so it is likely that the slightly elevated recombination current in the GO-based devices reflects the inhomogeneous edges and occasionally exposed ITO characteristic of the LB deposited film. Future work will focus on reducing these inhomogeneities.

Despite the comparable PCE performance of the present OPVs fabricated with GO or PEDOT:PSS IFLs, these results show that the GO-derived devices are significantly more durable. The accelerated lifetime testing results in Figure 5 clearly

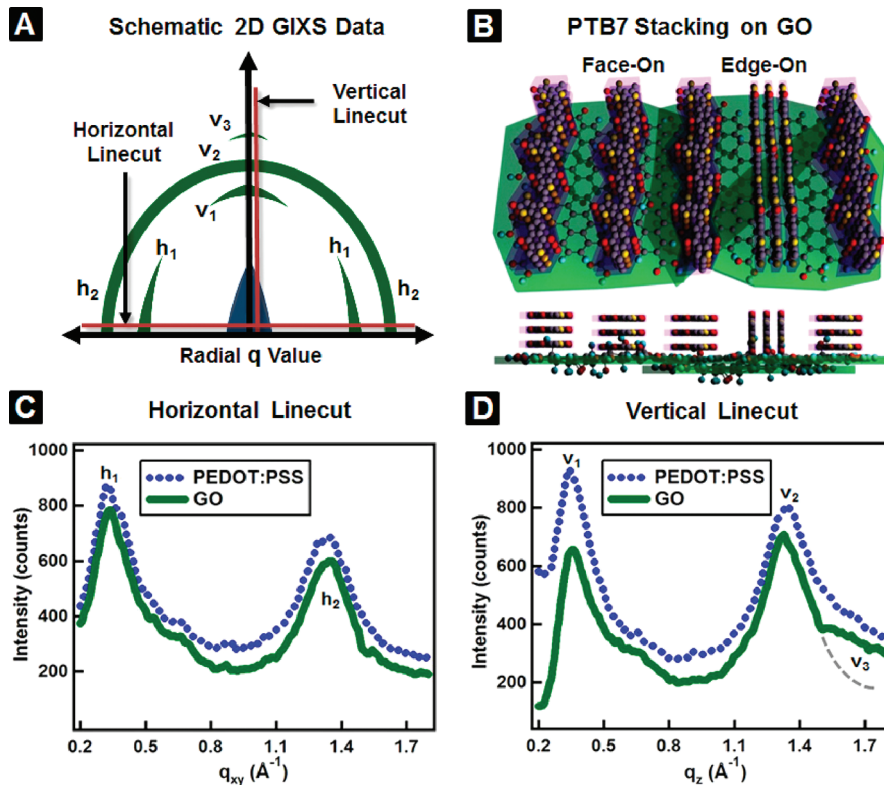


Figure 3. GIXS characterization of OPV active layer microstructures. (a) Schematic of raw 2D GIXS data and processing procedure for comparing signal intensities from multiple substrates, irradiated for equal times (see Supporting Information for complete 2D intensity maps). (b) Structural model from GIXS data showing preferential face-on π -stacking on ITO/GO substrates. (c) Horizontal linecuts from the 2D GIXS data collected for PTB7:PC₇₁BM films on ITO/PEDOT:PSS and ITO/GO substrates. (d) Vertical linecuts from the same 2D GIXS scans shown in panel c. Dashed gray line represents expected Gaussian decay.

demonstrate the limitations of PEDOT:PSS IFLs. In the accelerated thermal lifetime testing (Figure 5a), the observed initial efficiency loss is likely related to trapped H₂O and O₂ in the active layer and PEDOT:PSS.¹¹ After a smaller initial efficiency drop-off in the devices fabricated with GO IFLs, slower degradation in the linear regime leads to an overall 5-fold enhancement in PCE retention. In testing in which unencapsulated OPVs are exposed to ambient conditions at 80% relative humidity, the hygroscopic nature of PEDOT:PSS facilitates rapid transport of water into such devices.¹¹ This severely erodes OPV performance in hours, whereas the GO IFL devices survive for a 20-fold longer time period. The long time scale degradation of the GO devices is likely associated with edge-in diffusion through the active layer rather than an IFL-mediated failure mechanism.^{8,12,36}

The results of this work demonstrate the attraction of electrically tuned GO as an effective IFL for templating the optimum donor polymer π -stacking orientation for high efficiency OPVs. In addition to functioning as a solution-processable PEDOT:PSS alternative, GO significantly enhances the durability of fully fabricated devices by increasing the active layer–IFL interfacial stability under thermal and environmental stress. These advances should lead to further refinement of GO as a scalable, substrate-general material for a variety of optoelectronic applications.^{37–39}

■ EXPERIMENTAL SECTION

Substrate Preparation. Patterned ITO on glass ($10 \Omega/\square$) was purchased from Thin Film Devices with two electrically separated 3 mm anode strips. Substrates were cleaned via sonication

in several solvents followed by UV-ozone (UVO) treatment (see Supporting Information).

PEDOT:PSS Deposition. As-received PEDOT:PSS suspensions (Clevios 4083) were spin-coated onto the cleaned, UVO-treated ITO substrates at 5000 rpm for 30 s (thickness ~ 40 nm), and then annealed on a hot plate at 150 °C for 15 min in air. Substrates were then transferred to a glovebox immediately after annealing to minimize water condensation on the surface.

GO Synthesis and Deposition. GO was prepared from graphite powder (Bay Carbon, SP-1) using a modified Hummers procedure.⁴⁰ GO was deposited onto the substrates using the LB transfer technique as previously reported.³² Briefly, the as-prepared GO was suspended in a 1:5 water/methanol solution and spread dropwise onto the water surface in an LB trough (Nima Technology, model 116). Substrates were then immersed in the trough, and the film was compressed by barriers at a speed of 50 cm²/min until a surface pressure of ~ 25 –30 mN/m was reached, as measured by a Whelmy plate. The GO monolayer was then transferred to the substrates by vertically raising the sample at a speed of 2 mm/min.

Energy Level Tuning of GO. After LB deposition of GO, the films were annealed in air at 150 °C for 15 min to remove residual water and solvent from the film. Exposure to brief, low-level UVO treatment (~ 8 mW/cm²) was then used to tune the oxidation level of the GO flakes. This change was monitored by characterizing the hydrophobicity of the surface using advancing aqueous contact angle measurements. The optimum exposure time for device performance was correlated with the

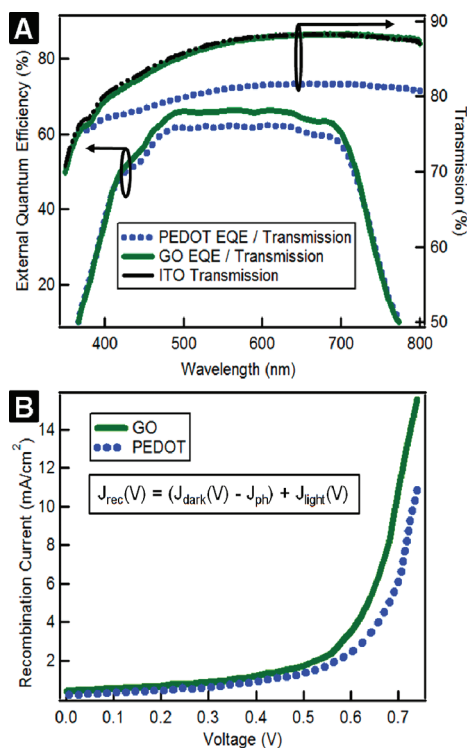


Figure 4. Optical transmission, EQE, and device recombination characteristics of OPVs using GO or PEDOT:PSS IFLs. (a) Optical spectra comparing the transmission characteristics of GO and PEDOT:PSS films overlaid on EQE measurements on the resulting devices. (b) Recombination current as a function of voltage for devices under illumination.

highest occupied MO energy of the donor polymer, suggesting that tuning the GO oxidation level also modifies the surface electronic properties (see Figure S7 for $J-V$ data comparing UVO exposure times for devices with PTB7 and poly(3-hexylthiophene) (P3HT) electron donating polymers).

Solar Cell Fabrication and Testing. The PTB7 polymer used in this work was synthesized according to previously reported methods.²⁰ The batch used for the 48 devices included in the present statistical analysis had $M_n = 42\,000$ and PDI = 2.2. In a flask, 10 mg of PTB7 and 15 mg of PC₇₁BM (American Dye Source) were dissolved in 0.97/0.03 (mL/mL) chlorobenzene/1,8-diodo-octane (Drisolv). The solution was stirred under N₂ overnight at 70 °C to ensure complete dissolution. Active layer films were then deposited by spin-casting at 1500 rpm after passing the solution through a 0.22 μm polytetrafluoroethylene (PTFE) filter. The still-wet films were immediately transferred from the spin-coater chuck to covered Petri dishes and allowed to dry undisturbed. While still in the glovebox, standard thermal evaporation of LiF/Al cathodes and epoxy encapsulation completed the fabrication of four 6.0 mm² devices on each substrate (see Supporting Information)

Device evaluation was performed at 298 K using a Class A Spectra-Nova Technologies solar cell analyzer with a Xe lamp that simulates AM1.5G light from 400 to 1100 nm. The instrument was calibrated with a monocrystalline Si diode fitted with a KG3 filter to bring spectral mismatch to unity. The calibration standard was calibrated by the National Renewable Energy Laboratory. Four-point contacts were made to the substrate with Ag paste and copper alligator clips. Individual devices were

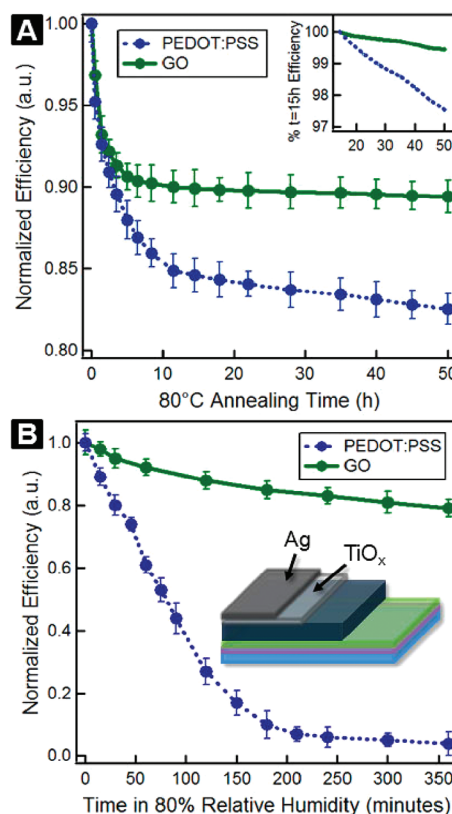


Figure 5. Durability characteristics of PTB7:PC₇₁BM solar cells with PEDOT:PSS and GO IFLs. (a) Thermal degradation of encapsulated devices at 80 °C under an N₂ atmosphere. Inset: Plot of the data between 15 and 50 h, as a percentage of the efficiency at $t = 15$ h. (b) Environmental degradation of unencapsulated devices fabricated with air-stable electrodes at 80% relative humidity and 25 °C. Inset: Schematic of the device geometry used for humidity degradation testing.

isolated by a mask during testing to avoid current collection from adjacent devices and edge effects.²⁶

GIXS Film Characterization. GIXS spectra were collected at Beamline 8ID of the Advanced Photon Source (APS) at Argonne National Laboratory. The scattering intensities are given as a function of the scattering vector, $q = 4\pi/l \sin \theta$, where θ is half the scattering angle and $l = 1.6868$ Å is the wavelength of the incident radiation. A 2D area Pilatus 100k detector was used to collect the spectra and was situated 200.4 mm from the sample. The films were illuminated at an incidence angle of about 0.2° by the X-rays at 7.35 keV. The angle of incidence was determined using X-ray reflectivity and chosen to be slightly larger than the critical angle of the film, but smaller than the critical angle of the substrate, so that the X-ray beam penetrated the entire film, but the background scattering from the substrate was minimized. Data were analyzed as described previously.²⁷

ASSOCIATED CONTENT

S Supporting Information. GO synthesis and film characterization with scanning electron microscopy, XPS, and Raman data collected for structural confirmation, GIXS data collection and processing methods, 2D plates from GIXS experiments, and current–voltage data from solar cells with varying exposure time to UVO. This material is available free of charge via the Internet at <http://pubs.acs.org>.

■ AUTHOR INFORMATION

Corresponding Author

*E-mail: lupingu@uchicago.edu (L.Y.); lchen@anl.gov (L.X.C.); t-marks@northwestern.edu (T.J.M.); m-hersam@northwestern.edu (M.C.H.).

■ ACKNOWLEDGMENT

We thank the ANSER Center, an Energy Frontier Research Center funded by the U.S. Department of Energy, Office of Science, Office of Basic Energy Sciences, under Award Number DE-SC0001059 for support of this research, and the NSF-MRSEC program through the Northwestern University Materials Research Science and Engineering Center for providing characterization facilities (DMR-0520513). J.H. and L.C. thank NSF-CAREER (Grant DMR 0955612) for support, and I.P.M. thanks the National Defense Science and Engineering Graduate Fellowship Program for fellowship support. This work utilized public facilities within the NUANCE Center, which is supported by the NSF-NSEC, NSF-MRSEC, Keck Foundation, State of Illinois, and Northwestern University. We also thank J. Servaites, B. Savoie, D. Herman, and J. Wang for helpful discussions.

■ REFERENCES

- (1) Helgesen, M.; Sondergaard, R.; Krebs, F. C. Advanced Materials and Processes for Polymer Solar Cell Devices. *J. Mater. Chem.* **2010**, *20*, 36–60.
- (2) Brabec, C. J.; Gowrisanker, S.; Halls, J. J. M.; Laird, D.; Jia, S. J.; Williams, S. P. Polymer–Fullerene Bulk-Heterojunction Solar Cells. *Adv. Mater.* **2010**, *22*, 3839–3856.
- (3) (a) Servaites, J. D.; Ratner, M. A.; Marks, T. J. Organic Solar Cells: A New Look at Traditional Models. *Energy Environ. Sci.* **2011**, *4*, 4410–4422. (b) Kippelen, B.; Bredas, J. L. Organic Photovoltaics. *Energy Environ. Sci.* **2009**, *2*, 251–261.
- (4) Seo, J. H.; Gutacker, A.; Sun, Y. M.; Wu, H. B.; Huang, F.; Cao, Y.; Scherf, U.; Heeger, A. J.; Bazan, G. C. Improved High-Efficiency Organic Solar Cells via Incorporation of a Conjugated Polyelectrolyte Interlayer. *J. Am. Chem. Soc.* **2011**, *133*, 8416–8419.
- (5) Loser, S.; Bruns, C. J.; Miyauchi, H.; Ortiz, R. O. P.; Facchetti, A.; Stupp, S. I.; Marks, T. J. A Naphthodithiophene-Diketopyrrolopyrrole Donor Molecule for Efficient Solution-Processed Solar Cells. *J. Am. Chem. Soc.* **2011**, *133*, 8142–8145.
- (6) He, F.; Wang, W.; Chen, W.; Xu, T.; Darling, S. B.; Strzalka, J.; Liu, Y.; Yu, L. Tetrathienoanthracene-Based Copolymers for Efficient Solar Cells. *J. Am. Chem. Soc.* **2011**, *133*, 3284–3287.
- (7) Hauch, J. A.; Schilinsky, P.; Choulis, S. A.; Childers, R.; Biele, M.; Brabec, C. J. Flexible Organic P3HT:PCBM Bulk-Heterojunction Modules with More Than 1 Year Outdoor Lifetime. *Sol. Energy Mater. Sol. Cells* **2008**, *92*, 727–731.
- (8) Lloyd, M. T.; Peters, C. H.; Garcia, A.; Kauvar, I. V.; Berry, J. J.; Reese, M. O.; McGehee, M. D.; Ginley, D. S.; Olson, D. C. Influence of the Hole-Transport Layer on the Initial Behavior and Lifetime of Inverted Organic Photovoltaics. *Sol. Energy Mater. Sol. Cells* **2011**, *95*, 1382–1388.
- (9) Paci, B.; Generosi, A.; Bailo, D.; Rossi Albertini, V.; de Bettignies, R. Discriminating Bulk, Surface and Interface Aging Effects in Polymer-Based Active Materials for Efficient Photovoltaic Devices. *Chem. Phys. Lett.* **2010**, *494*, 69–74.
- (10) Sun, Y. M.; Takacs, C. J.; Cowan, S. R.; Seo, J. H.; Gong, X.; Roy, A.; Heeger, A. J. Efficient, Air-Stable Bulk Heterojunction Polymer Solar Cells Using MoO(x) as the Anode Interfacial Layer. *Adv. Mater.* **2011**, *23*, 2226–2230.
- (11) Girtan, M.; Rusu, M. Role of ITO and PEDOT:PSS in Stability/Degradation of Polymer:Fullerene Bulk Heterojunctions Solar Cells. *Sol. Energy Mater. Sol. Cells* **2010**, *94*, 446–450.
- (12) Lloyd, M. T.; Olson, D. C.; Lu, P.; Fang, E.; Moore, D. L.; White, M. S.; Reese, M. O.; Ginley, D. S.; Hsu, J. W. P. Impact of Contact Evolution on the Shelf Life of Organic Solar Cells. *J. Mater. Chem.* **2009**, *19*, 7638–7649.
- (13) Conings, B.; Bertho, S.; Vandewal, K.; Senes, A.; D’Haen, J.; Manca, J.; Janssen, R. A. J. Modeling the Temperature Induced Degradation Kinetics of the Short Circuit Current in Organic Bulk Heterojunction Solar Cells. *Appl. Phys. Lett.* **2010**, *96*, 163301.
- (14) Reese, M. O.; Morfa, A. J.; White, M. S.; Kopidakis, N.; Shaheen, S. E.; Rumbles, G.; Ginley, D. S. Pathways for the Degradation of Organic Photovoltaic P3HT:PCBM Based Devices. *Sol. Energy Mater. Sol. Cells* **2008**, *92*, 746–752.
- (15) Jørgensen, M.; Norrman, K.; Krebs, F. C. Stability/Degradation of Polymer Solar Cells. *Sol. Energy Mater. Sol. Cells* **2008**, *92*, 686–714.
- (16) Li, S.-S.; Tu, K.-H.; Lin, C.-C.; Chen, C.-W.; Chhowalla, M. Solution-Processable Graphene Oxide as an Efficient Hole Transport Layer in Polymer Solar Cells. *ACS Nano* **2010**, *4*, 3169–3174.
- (17) Matyba, P.; Yamaguchi, H.; Chhowalla, M.; Robinson, N. D.; Edman, L. Flexible and Metal-Free Light-Emitting Electrochemical Cells Based on Graphene and PEDOT-PSS as the Electrode Materials. *ACS Nano* **2010**, *5*, 574–580.
- (18) Dreyer, D. R.; Park, S.; Bielawski, C. W.; Ruoff, R. S. The Chemistry of Graphene Oxide. *Chem. Soc. Rev.* **2010**, *39*, 228–240.
- (19) Loh, K. P.; Bao, Q.; Eda, G.; Chhowalla, M. Graphene Oxide as a Chemically Tunable Platform for Optical Applications. *Nat. Chem.* **2010**, *2*, 1015–1024.
- (20) Liang, Y. Y.; Feng, D. Q.; Wu, Y.; Tsai, S. T.; Li, G.; Ray, C.; Yu, L. P. Highly Efficient Solar Cell Polymers Developed via Fine-Tuning of Structural and Electronic Properties. *J. Am. Chem. Soc.* **2009**, *131*, 7792–7799.
- (21) Liang, Y.; Xu, Z.; Xia, J.; Tsai, S. T.; Wu, Y.; Li, G.; Ray, C.; Yu, L. For the Bright Future-Bulk Heterojunction Polymer Solar Cells with Power Conversion Efficiency of 7.4%. *Adv. Mater.* **2010**, *22*, 135–138.
- (22) Hains, A. W.; Marks, T. J. High-Efficiency Hole Extraction/Electron-Blocking Layer to Replace Poly(3,4-ethylenedioxythiophene):Poly(styrene sulfonate) in Bulk-Heterojunction Polymer Solar Cells. *Appl. Phys. Lett.* **2008**, *92*, 023504.
- (23) Irwin, M. D.; Buchholz, D. B.; Hains, A. W.; Chang, R. P. H.; Marks, T. J. p-Type Semiconducting Nickel Oxide as an Efficiency-Enhancing Anode Interfacial Layer in Polymer Bulk-Heterojunction Solar Cells. *Proc. Natl. Acad. Sci. U.S.A.* **2008**, *105*, 2783–2787.
- (24) Hains, A. W.; Liu, J.; Martinson, A. B. F.; Irwin, M. D.; Marks, T. J. Anode Interfacial Tuning via Electron-Blocking/Hole-Transport Layers and Indium Tin Oxide Surface Treatment in Bulk-Heterojunction Organic Photovoltaic Cells. *Adv. Funct. Mater.* **2010**, *20*, 595–606.
- (25) Irwin, M. D.; Liu, J.; Leever, B. J.; Servaites, J. D.; Hersam, M. C.; Durstock, M. F.; Marks, T. J. Consequences of Anode Interfacial Layer Deletion. HCl-Treated ITO in P3HT:PCBM-Based Bulk-Heterojunction Organic Photovoltaic Devices. *Langmuir* **2010**, *26*, 2584–2591.
- (26) Irwin, M. D.; Servaites, J. D.; Buchholz, D. B.; Leever, B. J.; Liu, J.; Emery, J. D.; Zhang, M.; Song, J. H.; Durstock, M. F.; Freeman, A. J.; et al. Structural and Electrical Functionality of NiO Interfacial Films in Bulk Heterojunction Organic Solar Cells. *Chem. Mater.* **2011**, *23*, 2218–2226.
- (27) Guo, J. C.; Liang, Y. Y.; Szarko, J.; Lee, B.; Son, H. J.; Rolczynski, B. S.; Yu, L. P.; Chen, L. X. Structure, Dynamics, and Power Conversion Efficiency Correlations in a New Low Bandgap Polymer:PCBM Solar Cell. *J. Phys. Chem. B* **2010**, *114*, 4746–4746.
- (28) Szarko, J. M.; Guo, J.; Liang, Y.; Lee, B.; Rolczynski, B. S.; Strzalka, J.; Xu, T.; Loser, S.; Marks, T. J.; Yu, L.; et al. When Function Follows Form: Effects of Donor Copolymer Side Chains on Film Morphology and BHJ Solar Cell Performance. *Adv. Mater.* **2010**, *22*, 5468–5472.
- (29) Cates, N. C.; Gysel, R.; Dahl, J. E. P.; Sellinger, A.; McGehee, M. D. Effects of Intercalation on the Hole Mobility of Amorphous Semiconducting Polymer Blends. *Chem. Mater.* **2010**, *22*, 3543–3548.
- (30) Cote, L. J.; Kim, J.; Zhang, Z.; Sun, C.; Huang, J. Tunable Assembly of Graphene Oxide Surfactant Sheets: Wrinkles, Overlaps and Impacts on Thin Film Properties. *Soft Matter* **2010**, *6*, 6096–6099.

- (31) Kim, F.; Cote, L. J.; Huang, J. Graphene Oxide: Surface Activity and Two-Dimensional Assembly. *Adv. Mater.* **2010**, *22*, 1954–1958.
- (32) Cote, L. J.; Kim, F.; Huang, J. Langmuir–Blodgett Assembly of Graphite Oxide Single Layers. *J. Am. Chem. Soc.* **2008**, *131*, 1043–1049.
- (33) Yan, J.-A.; Xian, L.; Chou, M. Y. Structural and Electronic Properties of Oxidized Graphene. *Phys. Rev. Lett.* **2009**, *103*, 086802.
- (34) Lalic, S.; Inganäs, O. Modeling Electrical Transport in Blend Heterojunction Organic Solar Cells. *J. Appl. Phys.* **2005**, *97*, 124901.
- (35) Park, S. H.; Roy, A.; Beaupre, S.; Cho, S.; Coates, N.; Moon, J. S.; Moses, D.; Leclerc, M.; Lee, K.; Heeger, A. J. Bulk Heterojunction Solar Cells with Internal Quantum Efficiency Approaching 100%. *Nat. Photonics* **2009**, *3*, 297–302.
- (36) Norrman, K.; Madsen, M. V.; Gevorgyan, S. A.; Krebs, F. C. Degradation Patterns in Water and Oxygen of an Inverted Polymer Solar Cell. *J. Am. Chem. Soc.* **2010**, *132*, 16883–16892.
- (37) Yong, V.; Tour, J. M. Theoretical Efficiency of Nanostructured Graphene-Based Photovoltaics. *Small* **2010**, *6*, 313–318.
- (38) Klare, J. E.; Murray, I. P.; Goldberger, J.; Stupp, S. I. Assembling p-Type Molecules on Single Wall Carbon Nanotubes for Photovoltaic Devices. *Chem. Commun.* **2009**, 3705–3707.
- (39) Tung, V. C.; Kim, J.; Cote, L. J.; Huang, J. Sticky Interconnect for Solution-Processed Tandem Solar Cells. *J. Am. Chem. Soc.* **2011**, *133*, 9262–9265.
- (40) Hummers, W. S.; Offeman, R. E. Preparation of Graphitic Oxide. *J. Am. Chem. Soc.* **1958**, *80*, 1339–1339.